Analysis of the Steady-State Axial Flow in the Hall Thruster

Avi Cohen-Zur[†], Amnon Fruchtman[‡], Joseph Ashkenazy[*], and Alon Gany[†]
[†] *Faculty of Aerospace Engineering, Technion - Israel Institute of Technology, Haifa 32000, Israel, 972-48294964, aerbnac@aerodyne.technion.ac.il*
[‡] *Holon Academic Institute of Technology, P.O. Box 305, Holon 58102, Israel, 972-35026617, fnfrucht@hait.ac.il*
[*] *Propulsion Physics Laboratory, Soreq NRC, Yavne 81800, Israel, 972-89434543, Joseph@soreq.gov.il*

IEPC-01-26

[1] **The plasma flow in a Hall thruster is analyzed at the limit of intense full ionization. Momentum and energy balance is used to obtain analytical expressions for the current utilization, for the magnitude of the ion backflow current into the anode, and for the location of the ionization region along the channel. Also, axial profiles of flow variables for various input parameters are found by a numerical calculation, that is guided by the analytical expressions.**

I. Introduction

Hall thrusters [1]- [3] perform with efficiencies of more than 50% in the important range of specific impulses of 1500-2500 seconds. There is a substantial interest in improving the thruster performance in terms of a better plume collimation, operation extending to both higher and lower regimes of power and thrust, and variable thrust. Understanding the structure of the plasma flow in the thruster could be useful for accomplishing this task. In recent years we have developed a one-dimensional steady-state model of the Hall thruster and have demonstrated that flows with a smooth transition to supersonic velocities inside the thruster channel are possible [4]- [7]. We have also suggested how to deliberately generate an abrupt sonic transition inside the channel [7]. Additional aspects of the sonic transition have been addressed by other scientists [8]- [10].

Recently, Ahedo, Martinez-Cerezo, and Martinez-Sanchez [11] have found, for the first time theoretically, a steady-state flow that includes a backflow towards the anode, similar to the backflow claimed in the past [12]- [13]. The backflow results from the requirement that the Bohm condition [14] be satisfied at the anode. The calculation has been made for a set of parameter values that corresponds to the SPT-100 thruster [15]. In addition to the numerical calculation, relations between various flow parameters have been derived through an asymptotic analysis, for cases such as the case solved numerically, in which an intense full ionization is located at a small region along the channel.

In this paper we too address the thruster at the parameter regime of an intense full ionization. We adopt the boundary condition used in [11] and the resulting backflow towards the anode. Rather than calculating the flow for one set of parameter values only, we derive analytically expressions for the approximate current utilization, backflow current, and location of the ionization zone, as a function of the gas mass flow rate, applied voltage, magnetic field profile and thruster geometry. The analytical expressions are obtained by applying momentum and energy conservation laws. Also, axial profiles of flow variables for various flow parameters are found by a numerical calculation, that is guided by the analytical results.

In Sec. II we present the model. The analytical expressions are derived in Sec. III. Analytical and numerical results are presented in Sec. IV. The results are discussed in Sec. V.

II. The Model

The ion dynamics is governed by the continuity equation

$$\frac{d}{dz}(nv_i) = \frac{d}{dz}(nv_e) = -\frac{d}{dz}(n_a v_a) = S, \qquad (1)$$

and by the momentum equation

$$\frac{d}{dz}(m_i n v_i^2) = -en\frac{d\phi}{dz}\ , \qquad (2)$$

where n and n_a are the densities of the quasi-neutral plasma and neutral gas, v_i , v_e , and v_a are the ion, electron, and neutral velocities, e and m_i are the ion (xenon) charge and mass, S is the plasma source, and ϕ is the electrostatic potential. We assume that the main variation in the coaxial geometry of the thruster is along z, the axial coordinate. The ions are assumed cold, collisionless and unmagnetized.

The axial component of the electron momentum equation is

$$0 = en\frac{d\phi}{dz} - \frac{d\left(nT\right)}{dz} - j_\theta B \ , \tag{3}$$

where T is the electron temperature, j_θ is the electron azimuthal current density, B is the intensity of the approximately radial magnetic field, and the electron inertia is neglected. Adding Eqs. (2) and (3) and employing Ampere's law, $\left(B/\mu_0\right)\left(dB/dz\right) = j_\theta B$ (μ_0 is the permeability of free space), we obtain the momentum balance equation.

$$\frac{d}{dz}\left(m_i n v_i^2 + nT + \frac{B^2}{\mu_0}\right) = 0 \ , \tag{4}$$

which expresses the conservation of the total particle and electromagnetic pressure along the thruster. In the quasi-neutral plasma the electric-field pressure is negligible relative to the magnetic-field pressure. From the θ component of the electron momentum equation we obtain $j_\theta B = m_e\omega_c^2\Gamma_e/\nu$. Here m_e, ω_c, ν and $\Gamma_e \equiv nv_e$ are the electron mass, cyclotron frequency, collision frequency and flux density. It is assumed that $\nu \ll \omega_c$. The more useful form of the momentum balance equation is

$$\frac{d}{dz}\left(m_i n v_i^2 + nT\right) = -\frac{m_e\omega_c^2\Gamma_e}{\nu} \ . \tag{5}$$

The change in the particle total pressure is due to the gradient in the magnetic-field pressure.

The equation that governs the evolution of the electron enthalpy is

$$nv_e\frac{d}{dz}\left(\frac{5}{2}T\right) = env_e\frac{d\phi}{dz} - S(\alpha_i\epsilon_i + \frac{5}{2}T), \tag{6}$$

where ϵ_i is the ionization energy and $\alpha_i\epsilon_i$ is the average energy cost for ionization ($\epsilon_i = 12.1$ eV and $\alpha_i = 2.5$ for xenon). Wall losses, recombination and heat conduction are neglected. Multiplying Eq. (2) by v_i and adding the resulting equation to Eq. (6), we obtain an equation for the total energy balance.

$$\frac{d}{dz}\left(\frac{m_i n v_i^3}{2} + \frac{5}{2}nv_eT + nv_i\alpha_i\epsilon_i + j_T\phi\right) = S\left[\frac{m_i v_i^2}{2} - m_i v_i\left(v_i - v_a\right)\right] \ , \tag{7}$$

where $j_T \equiv en\left(v_i - v_e\right)$ is the total current density.

In the next section we derive approximate analytical expressions.

III. Analytical Expressions

We assume that the mass flow rate density and the applied voltage are large enough so that the ionization is intense and occurs inside a small region only. The channel is thus composed of a narrow ionization layer, an acceleration region between the ionization layer and the cathode (identified for simplicity with the exit plane), and a backflow region between the ionization layer and the anode. The division into regions and subregions has been demonstrated in Ref. [11]. At this limit of intense full ionization the electron flux density in the acceleration region is constant and equals the electron flux density from the cathode $\Gamma_e = \Gamma_{eC}$. In the backflow region $\Gamma_{eA} = \Gamma_{eC} - \dot{m}/(m_i A) + \Gamma_{iA}$, where $\dot{m}$ is the gas mass flow rate and A is the channel cross section, and Γ_{iA} is the ion flux density at the anode (that results from the backflow). Although more accurate approximations can be made, we here make a simplifying assumption and neglect the small ion momentum and electron pressure at the anode. Integrating Eq. (5) across the backflow region we obtain

$$\left(nT\right)_{il} = -m_e\Gamma_{eA}\int_0^{z_{il}} dz\nu_D \ . \tag{8}$$

Here il denotes the ionization layer, $z = 0$ is the location of the anode, and we adopt the notation of Ref. [11] $\nu_D \equiv \omega_c^2/\nu$. We neglect the small potential drops across the backflow region and across the ionization layer, so that the ion velocity at the cathode is $v_{iC} = v_0 \equiv \sqrt{2e\phi_A/m_i}$ (ϕ_A is the applied voltage). Neglecting also the small electron temperature at the cathode, we obtain by integrating Eq. (5) across the acceleration region:

$$\frac{\dot{m}}{A}v_0 - \left(nT\right)_{il} = -m_e\Gamma_{eC}\int_{z_{il}}^{L} dz\nu_D \ , \tag{9}$$

where L is the channel length and $z = L$ is the location of the cathode.

An additional relation is obtained from the equation for the total energy balance, by assuming that the ion "heating" due to ionization (the right hand side of Eq. (7)) is small. Integrating the equation along the channel yields:

$$\frac{\dot{m}}{Am_i}\left(e\phi_A + \alpha_i\epsilon_i\right) - \Gamma_{iA}\alpha_i\epsilon_i = j_T\phi_A. \qquad (10)$$

We use a third relation that is similar to that derived in Ref. [11]. In the acceleration region the ion and electron fluxes are constant. Equations (2) and (6) then yield $m_i v_i^2/2 + 5T/2 = e\phi_A$. At the sonic transition, that occurs at the edge of the ionization region [4]- [10], $m_i v_s^2/2 = 5T_s/6$ (quantities at the sonic transition layer are denoted by the subscript s). Therefore $T_s = 3e\phi_A/10$ and $v_s = \sqrt{e\phi_A/\left(2m_i\right)} = v_0/2$. Since a smooth sonic transition requires that ionization there is not zero, this transition has to occur close to the ionization layer, and $n_s\left(m_i v_i^2 + T\right)_s = \left(nT\right)_{il}$. Substituting $n_s = \dot{m}/\left(Am_i v_s\right)$ and $\left(m_i v_i^2 + T\right)_s = \left(4/5\right)e\phi_A$ into this last equation yields the sought-after third relation

$$\left(nT\right)_{il} = \frac{4}{5}\frac{\dot{m}}{A}v_0 \ . \qquad (11)$$

We therefore have three relations, which we write in the following dimensionless forms:

$$\frac{1}{5} = \left(J_T - 1\right)F(1-f) \ , \qquad (12)$$

$$\frac{4}{5} = \left(J_T + |J_{bf}|\right)Ff \ , \qquad (13)$$

$$\left(1 + \frac{\alpha_i\epsilon_i}{e\phi_A}\right) + |J_{bf}|\,\frac{\alpha_i\epsilon_i}{e\phi_A} = J_T \ . \qquad (14)$$

We used the definitions:

$$F \equiv \int_0^L dz\frac{m_e}{m_i}\frac{\nu_D}{v_0}, \quad f \equiv \frac{1}{F}\int_0^{z_{il}} dz\frac{m_e}{m_i}\frac{\nu_D}{v_0}, \qquad (15)$$

and

$$J_\alpha \equiv \frac{j_\alpha A m_i}{e\dot{m}}, \qquad \alpha = T,\ bf, \qquad (16)$$

where $j_{bf} \equiv e\Gamma_{iA}$ and in the case of a full ionization we discuss here j_T is

$$j_T = \left(\frac{e\dot{m}}{Am_i} - e\Gamma_{eC}\right). \qquad (17)$$

Equations (12), (13) and (14) determine J_T, $|J_{bf}|$ and f as functions of F and $\alpha_i\epsilon_i/\left(e\phi_A\right)$. We note that usually F is not really an input parameter since ν_D depends on J_{bf}, as we discuss shortly.

The efficiency turns out to be

$$\eta_T = \frac{1}{J_T} \ . \qquad (18)$$

IV. Numerical and Analytical Results

In this section we present analytical and numerical descriptions of the flow in the thruster. We start by presenting a numerical calculation of the flow for a set of parameter values that corresponds to the SPT-100 thruster [15], similar to the calculation first presented in Ref. [11]. The calculation demonstrates the features of the plasma flow at the limit of intense ionization, features that indeed justify the approximations that lead to the analytical results. We then present the analytical results that are obtained from the analytical expressions presented in the previous section. Finally, we present two additional numerical examples that exhibit the flow characteristics predicted by the analytical results.

In the calculation we employ the following nondimensional variables: $\zeta \equiv z/L$, $J \equiv nv_i m_i A/\dot{m}$, $V = v_i/v_0$, $\psi \equiv \phi/\phi_A$, $C_s^2 = \left(5/3\right)T_e/\left(m_i v_0^2\right)$. The boundary conditions are: $V = -C_s$ and $\psi = 1 + \psi_{sh}$ at the anode, $\zeta = 0$, and $T_e = T_{e,cathode}$ and $\psi = 0$ at the cathode, $\zeta = 1$. Here ψ_{sh} , the normalized potential drop across the anode sheath, depends on the electron temperature at the anode. We numerically solve Eqs. (1), (2), (5), and (6) with the above boundary conditions, by integrating the equations from the sonic transition plane towards both anode and cathode, as described in [4,5,7]. In Figure 1 we present the profiles of the flow variables for the parameters of the SPT-100. The results are similar to the results in Ref. [11], although, for simplicity, we assume a constant cross section flow. The magnetic field profile is shown in Fig. 1(i) and was taken as:

$$\frac{B}{B_{\max}} = \exp\left[-\frac{\left(\zeta - \zeta_m\right)^2}{\left(L_m/L\right)^2}\right] \ , \qquad (19)$$

with $\zeta_m = 0.4$ and $L_m = 20$ mm. The normalized total current and the total efficiency for this case are found to be $J_T \cong 1.163$ and $\eta_T \cong 1/J_T \cong 0.85$.

As pointed out in [11], the division into three major regions is apparent: a diffusion region including the anode presheath, with slow ion backflow, low electron temperature and very low electric field, a relatively narrow, intense ionization layer causing the electron temperature to drop (anodewise) sharply and the ion current to increase nearly to the maximal value possible (at full ionization), and an acceleration region in which the plasma is almost completely ionized and accelerates to almost the maximal velocity available by the applied voltage. The narrow ionization layer is placed between a low temperature region at the anode side and a no neutral region at the cathode side. This can be seen in Figs. 1(d),(f), & (h). The sonic plane is placed near the downstream edge of the ionization layer where the ionization rate is just sufficiently high to meet the regularity condition for a smooth sonic transition. The close-to-unity propellant and energy utilizations, $J = 1$ and $V = 1$ at the anode, are exhibited, supporting the approximations made in deriving the analytical expressions.

In the calculation anomalous colisionality had to be invoked. Similarly to [11] we chose Bohm diffusion with the Bohm parameter $\alpha_B = 1/80$. From the numerical results it follows that electron-neutral (e-n) and electron-ion (e-i) collisions are small relative to the anomalous collisions as seen in Fig. 1(h), in which the $\nu_{D,n}$ profile ($\nu_{D,n} \equiv \nu_D\ m_e/m_i$) follow closely the magnetic field profile. Thus, in the solution of the analytical model, we neglect e-n and e-i collisions, making ν_D a function of the magnetic field only. Therefore, F becomes an input parameter and f turns out to be a function of the axial coordinate z solely. The location of the sonic plane z_s is found once the value of f is determined.

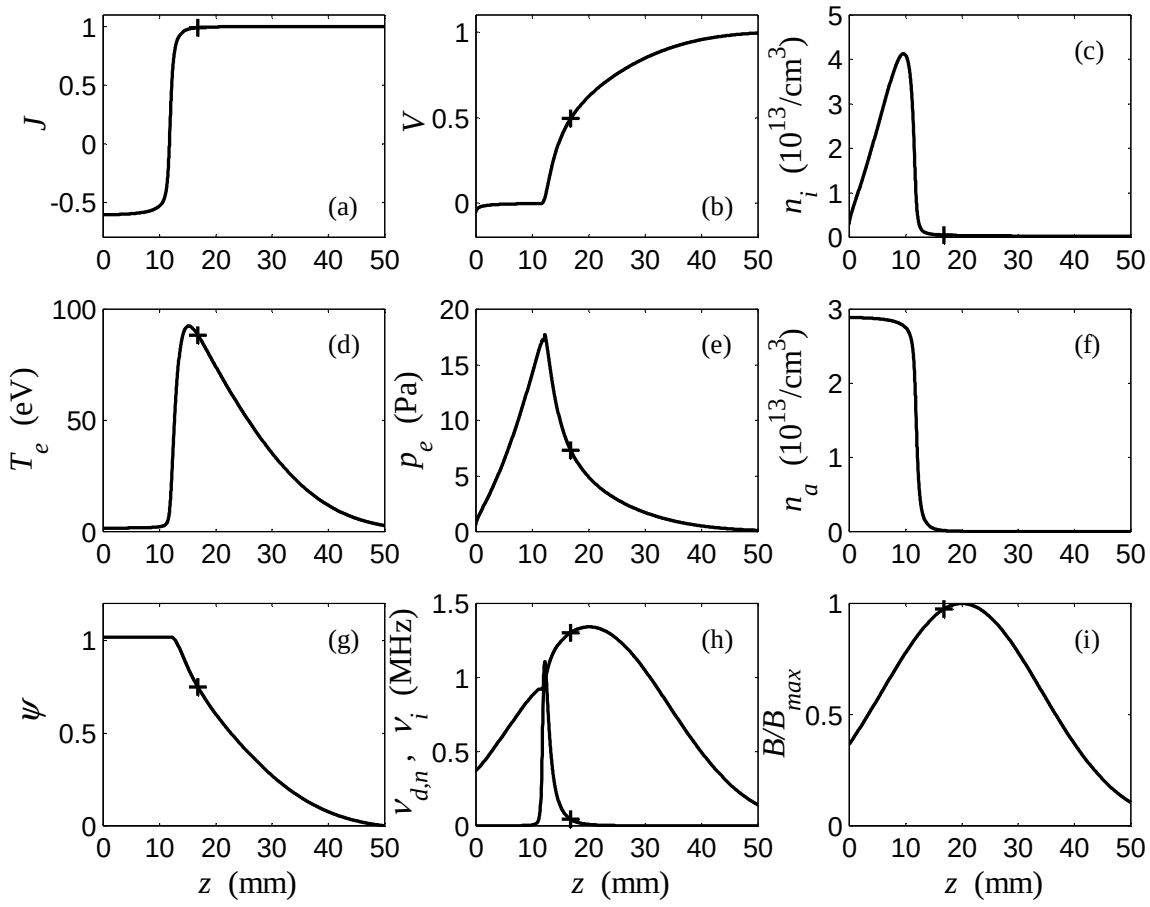

FIG. 1. Calculated profiles of flow variables in the Hall thruster: $A = 45$ cm^2,$L = 50$ mm, $\dot{m} = 5.32$ mg/s, $\phi_A = 300$ V, $B_{max} = 230$ G. The sonic transition location z_s is marked.

We turn now to the discussion of the analytical model. For a given profile of the magnetic field, the applied voltage and the maximal intensity of the magnetic field ($B_{\max}$), determine the parameter space. Equations (12)-(14) are solved for J_T , z_s , and J_{bf} for the specified profile of the magnetic field, as functions of given $B_{\max}$ and ϕ_A. It emerges from the analytical solution, that the location of the sonic transition depends on the applied voltage as well as on the magnetic field axial profile but not on $B_{\max}$. Results of the asymptotic model are presented in Figures 2-4 as contour maps of J_T , η_T , and J_{bf} on the parametric plane. The location of the sonic transition z_s is shown in Fig. 5 as a function of the applied voltage.

As seen in Fig. 2 the total current decreases as B_{max} is increased, as expected, since B_{max} impedes the electron axial motion. On the other hand, increasing the applied voltage decreases the efficiency and J_T is increased. This is the result of the additional power needed to ionize the higher ion backflow, as seen in Fig. 4. The location of the sonic transition plane (Fig. 5) moves towards the anode as the applied voltage increases. For each value of the applied voltage there exists a magnetic field for which J_{bf} vanishes. At this point J_T is the minimal possible and η_T is maximal for that ϕ_A. No steady state solutions exist for higher magnetic field intensities. The line of zero J_{bf} bounds the region of solution existence on the contour maps. The minimal total current satisfies the relation:

$$J_{T,min} = 1 + \frac{\alpha_i \epsilon_i}{e\phi_A} \ . \tag{20}$$

The same trends of dependencies of the total current, sonic plane location and ion backflow current are observed in the numerical solution of the full model. In Figure 6, we compare certain flow profiles of the previous case with two additional cases; a case of lower magnetic field intensity and a case of higher applied voltage. The neutral density is higher in both additional cases. This is explained by the higher ion backflow which recombines at the anode and joins the neutral gas flow. In both additional cases the total efficiency turns out to be lower. The total current and efficiency are found to be $J_T \cong 1.342$ and $\eta_T \cong 0.72$ in the case of lower magnetic field intensity, while in the high applied voltage case the values are $J_T \cong 1.192$ and $\eta_T \cong 0.82$.

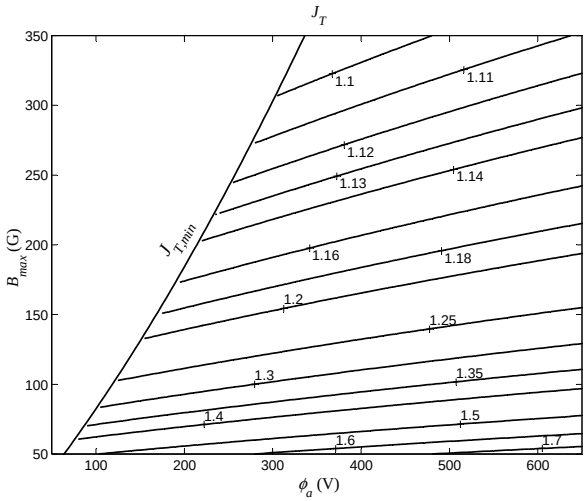

FIG. 2. Contours of equal J_T in the $\phi_A - B_{max}$ plane.

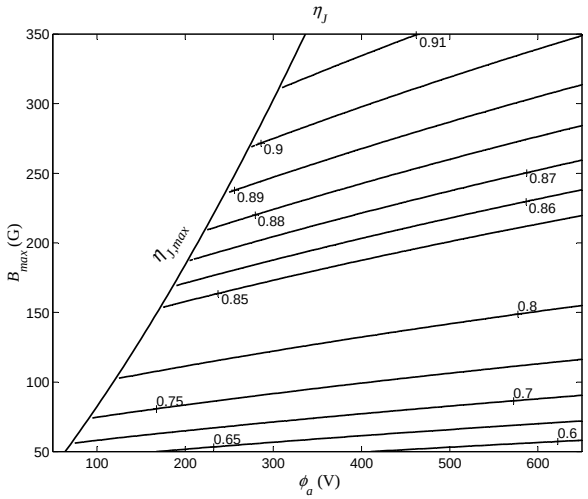

FIG. 3. Contours of thruster efficiency η_T in the $\phi_A - B_{max}$ plane ($\eta_J \equiv \eta_T$).

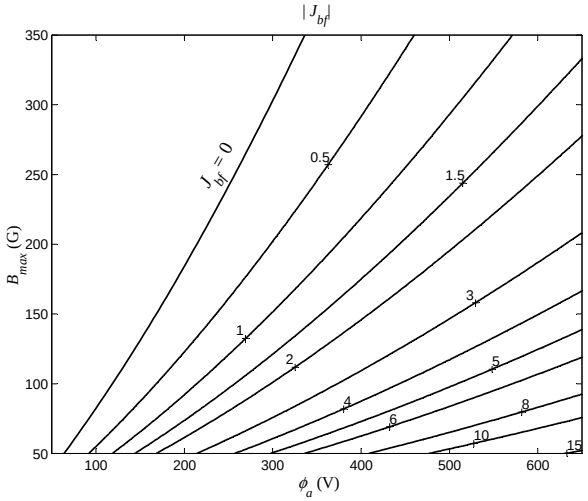

FIG. 4. Contours of ion backflow current in the $\phi_A - B_{max}$ plane.

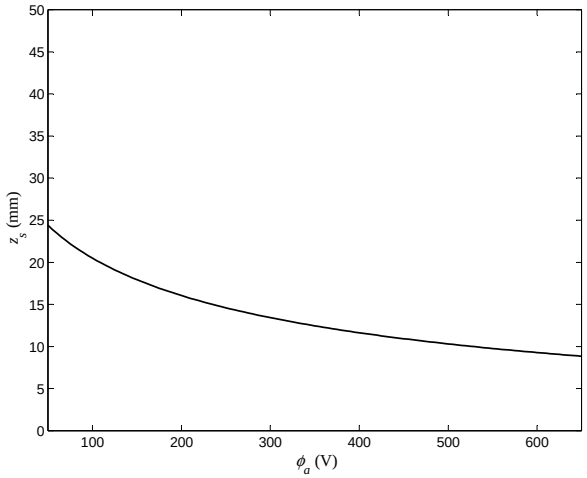

FIG. 5. The location of the sonic transition plane as a function of the applied voltage.

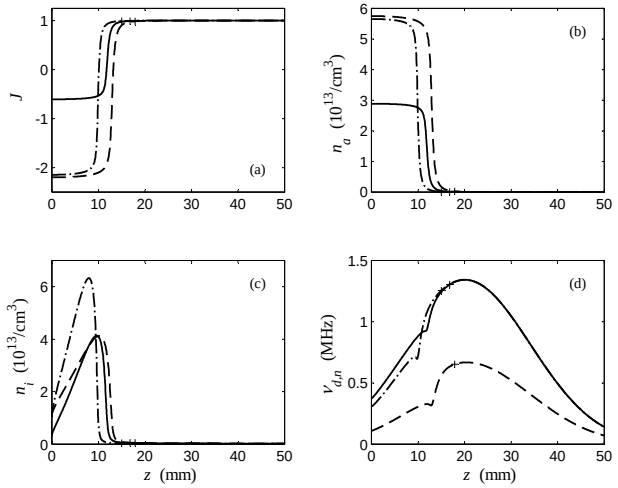

FIG. 6. Calculated profiles of flow variables for three cases: the previous case shown in Fig. 1 (solid line), a lower magnetic field case, $B_{max} = 115$ G (dashed line), and a higher applied voltage case, $\phi_A = 500$ V (dashed-dotted line).

V. Conclusion

The flow in the Hall thruster was analyzed at the limit of intense full ionization. The derived analytical expressions provide better understanding of the thruster behaviour and of the efficiency dependence on the input parameters. The importance of the ion backflow, as an energy consuming mechanism, was recognized. The understanding gained by the analysis may be used in the search for improved thruster configurations. In future studies heat conductivity and ion loss in lateral walls may also be addressed. These effects may reduce the calculated efficiencies to more realistic values.

VI. Acknowledgements

The authors are grateful to Prof. N. J. Fisch and to Mr. G. Makrinich for helpful discussions. This research has been partially supported by the Israel Space Agency and by a Grant No. 9800145 from the United States-Israel Binational Science Foundation (BSF), Jerusalem, Israel.

[1] A. I. Morozov, Yu. V. Esipchuk, G. N. Tilinin, A. V. Trofinov, Yu. A. Sharov, and G. Ya. Shahepkin, Sov. Phys. Tech. Phys. **17**, 38 (1972).

[2] J. Ashkenazy, Y. Raitses, and G. Appelbaum, Phys. Plasmas **5**, 2055 (1998).

[3] V. V. Zhurin, H. R. Kaufman, and R. S. Robinson, Plasma Sources Sci. Technol. **8**, R1 (1999).

[4] A. Fruchtman, N.J. Fisch, J. Ashkenazy, and Y. Raitses, IEPC 97-022, *25th International Electric Propulsion Conference*, Cleveland, Ohio, Aug. 1997.

[5] A. Fruchtman and N. J. Fisch, AIAA paper 98-3500, *34th Joint Propulsion Conference*, Cleveland, OH 1998 (American Institute of Aeronautics and astronautics, Washington, DC, 1998).

[6] A. Cohen - Zur, A. Fruchtman, and J. Ashkenazy, IEPC 99-108, *26th International Electric Propulsion Conference*, Kitakyushu, Japan, 1999. .

[7] A. Fruchtman, N. J. Fisch, and Y. Raitses, Phys. Plasmas **8**, 2000 (2001).

[8] E. Ahedo and M. Martinez-Sanchez, AIAA paper 98-8788, *34th Joint Propulsion Conference*, Cleveland, OH 1998 (American Institute of Aeronautics and astronautics, Washington, DC, 1998).

[9] K. Makowski, Z. Peradzynski, N. Gascon and M. Dudeck, AIAA paper 99-2295, *35th Joint Propulsion Conference*, Los Angeles, CA 1999 (American Institute of Aeronautics and astronautics, Washington, DC, 1999).

[10] V. Yu. Fedotov, A. A. Ivanov, G. Guerrini, A. N. Vesselovzorov, and M. Bacal, Phys. Plasmas **6**, 4360 (1999).

[11] E. Ahedo, P. Martinez-Cerezo, and M. Martinez-Sanchez, Phys. Plasmas **8**, 3058 (2001).

[12] A. Bishaev and V. Kim, Sov. Phys. Tech. Phys. **23**, 1055 (1978).

[13] V. Kim, J. Propul. Power **14**, 736 (1998).

[14] D. Bohm, in "The characteristics of Electrical Discharges in Magnetic Fields", edited by A. Guthry and R. K. Wakerling.

[15] J. Sankovic, J. Hamley, and T. Hang, IEPC 93-094, 23th International Electric Propulsion Conference.